Molecular BioSystems

Accepted Manuscript

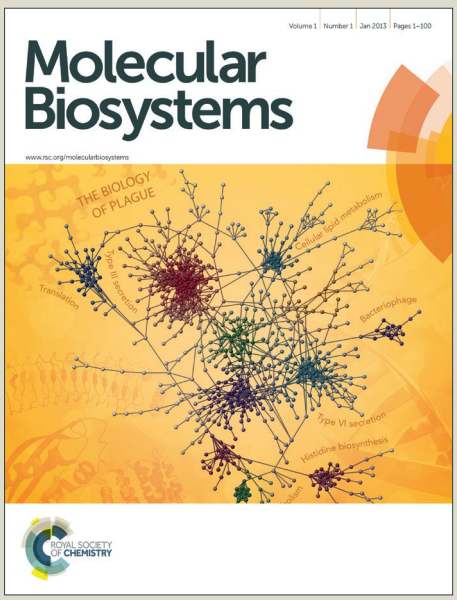

ROYAL SOCIETY OF CHEMISTRY

www.rsc.org/molecularbiosystems

Effect of T68A/N126Y mutations on conformational and ligand binding landscape of Coxsackievirus B3 3C protease

Soumendranath Bhakat*

Division of Biophysical Chemistry, Lund University, P.O. Box 124, SE-22100 Lund, Sweden
URL: https://cbiores.wordpress.com/

* Corresponding author: Soumendranath Bhakat, email: soumendranath.bhakat@bpc.lu.se
bhakatsoumendranath@gmail.com

Graphical Abstract

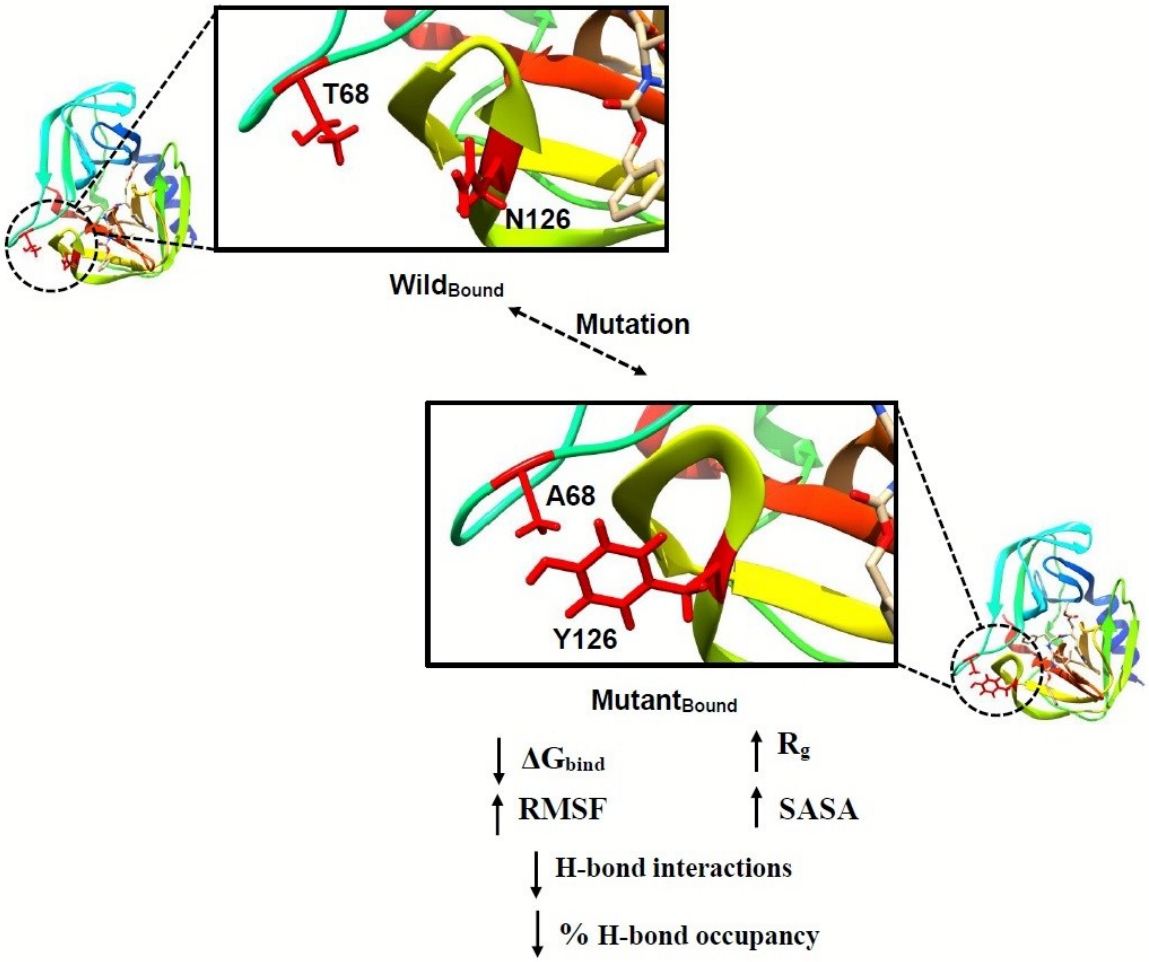

Abstract

3C protease of Coxsackievirus B3 (CVB3) plays an essential role in the viral replication cycle, and therefore, emerged as an attractive therapeutic target for the treatment of human diseases caused by CVB3 infection. In this study, we report the first account of the molecular impact of T68A/N126Y double mutant ($Mutant_{Bound}$) using an integrated computational approach. Molecular dynamics simulation and post-dynamics binding free energy, principle component analysis (PCA), hydrogen bond occupancy, SASA, R_g and RMSF confirms that T68A/N126Y instigated an increased conformational flexibility due to loss of intra and inter molecular hydrogen bond interactions and other prominent binding forces, which led to a decreased protease grip on ligand (3CPI). The double mutations triggered a distortion orientation of the 3CPI in the active site and decreases the binding energy, ΔG_{bind} (~3 kcal/mol) compared to the wild type ($Wild_{Bound}$). The van der Waals and electrostatic energy contributions coming from residue 68 and 126 are lower for $Mutant_{Bound}$ when compared with $Wild_{Bound.}$ In addition, variation in the overall enzyme motion as evident from the PCA, distorted hydrogen bonding network and loss of protein-ligand interactions resulted in loss of inhibitor efficiency. The comprehensive molecular insight gained from this study should be of great importance in understanding drug resistance against CVB3 3C protease also it will assist in the designing of novel coxsackievirus B3 inhibitors with high ligand efficacy on resistant strains.

Keywords: Coxsackie virus; 3C protease; T68A/N126Y mutations; resistance; molecular dynamics

1. Introduction

Picornaviruses are important human pathogenic viruses, which include enterovirus (EV), human poliovirus (HPV), hepatitis A virus (HAV), human rhinovirus (HRV), and Coxsackievirus (CV)(*1-5*). CVs are positive sense, single-stranded RNA viruses which are divided into two groups (Coxsackie A and Coxsackie B) (*6-9*). Each group is categorized into several serotypes. Once a person gets the virus, it takes an average of one to two days for symptoms to develop. People are most contagious in the first week of illness, but the virus may still be present up to one week after symptoms resolve. The virus persists longer in children and those whose immune systems are weak. It is also unaffected by the acids present in the stomach and can live on surfaces for a long period of time. Coxsackievirus A (CVA) virus causes paralysis and death, with extensive skeletal muscle necrosis (*10-12*). Coxsackievirus B (CVB) causes less severe infection in the mice, but with damage to more organ systems, such as heart, brain, liver, pancreas, and skeletal muscles. There are six groups of CVB serotypes (CVB1-6) within the Picornaviridae family (*13-15*).

Coxsackievirus B3 (CVB3) is a small (approximately 300 Å in diameter), non-enveloped, positive-stranded RNA enterovirus, associated with a number of diverse syndromes including viral myocarditis, hepatitis, pancreatitis, virus-induced heart disease and meningitis in humans (*8, 16-18*). CVB3 related diseases causes approximately 50% of the heart transplantations registered annually worldwide. The CVB3 genome is 7.4 kb long and contains untranslated regions (UTRs) at both its 5′ and 3′ ends (**Figure 1**) and a large open reading frame in between that encodes the viral polyprotein, which is processed into structural and nonstructural proteins by viral proteases. Upon infection, the positive-

strand RNA genome of CVB3 is translated into a large poly-protein precursor that is subject to successive proteolytic cleavage processes to generate functional and structural viral proteins. The proteolytic processing of poly-protein is essential for the production of new infectious virions and it is depends on two virally encoded proteases 2A and 3C protease (*19, 20*). In particular, the picornavirus 3C protease is required for the majority of proteolytic cleavage events during viral replication. Therefore these enzymes are attractive targets for the development of therapeutic antiviral agents because there are no effective therapeutic strategies for the prevention or treatment of diseases caused by CVB3.

Figure 1

Coxsackievirus B3 3C protease (CVB3 3CP) is highly homologous with the human rhinovirus (HRV) 3CP in amino acid sequence (approximately 64%). Therefore, *Matthews et al*. showed that Rupintrivir (novel HRV inhibitor) had activity against CVB3 enzyme with a half-maximal effective concentration (*21, 22*). Additional studies also indicated that a substitutions of the ethyl ester in position P2 of AG7088 (Rupintrivir) by large aromatic moieties will lead to a significant enhancement of affinity to the enzyme(*21*). This can be ascribed to the hydrophobic interaction with residue Tyr22 of the 3CPRO. *Soo-Hyeon Yun et al.* also reported a potent CVB3 3CP inhibitor (3CPI) using the backbone protein structure of AG7088, which showed viral proliferation in HeLa cells in vitro (*8*). Repetitive cultivation of the CVB3 3CP in the presence of rupintrivir raised two resistance mutations (T68A and N126Y) (*23*). The X-rays crystal analysis indicate that the structure of the T68A mutant is close to that of the wild-type enzyme, whereas the N126Y mutation apparently leads to major rearrangements of the

structure. However, details of how these changes affect the binding of inhibitors is yet to be reported. In literatures recombinant viruses harboring these mutations have been demonstrated to be resistant against rupintrivir(*23*).

In this work, we aim to provide a comprehensive understanding of the impact of the T68A and N126Y mutations (**Figure 2**) on the activity of inhibitors towards 3C Protease of Coxsackie virus B3. Findings from this study could be critical in future development of more potent Coxsackie Virus B3 inhibitors and understanding molecular basis of drug resistance. In recent years, molecular dynamics simulation and post dynamics analyses become the close counterpart of experiment in understanding molecular basis of drug resistance across a number of different biological systems (*24*). Different post-dynamics analyses have been widely used to gain an overall atomic level understanding from molecular dynamics simulations. Among these, per-residue C-α fluctuation, R_g, hydrogen bond occupancy and principal componenet analysis (PCA) emerged as an essential tool to understand the effect of mutation in conformational and ligand binding landscape of a biomolecule. It has also been studied that mutation(s) in a protein residue leads to the disruption in the protein backbone mainly due a decrease in intra-residue hydrogen bond connections.

Figure 2

Reports from this study highlights the effect of T68A/N126Y mutations on conformational and ligand binding landscape of 3C protease of CVB3 from a computational perspective. To the best of our knowledge, this is the first account of any such reports on the CVB3 which not only provides a valid computational model to

understand T68A/N126Y mutations but will also boost future drug discovery efforts to counter drug-resistance.

2. Computational methods

2.1. System preparation

In order to understand the effect of T68A/N126Y mutations on 3C protease of CVB3 the apo and ligand (Code named: 3CPI, the detailed IUPAC name of the ligand is presented in Supplementary Material) bound conformations of the viral protease was retrieved from protein data bank (**Table 1**). The α, β unsaturated ethyl ester, 3CPI complexed with bound conformation of CVB3 3C protease considered as a prototype ligand to understand the effect of mutations on drug/ligand binding landscape. All non-standard residues were removed and missing residues were adjusted using graphical user interface (GUI) of Chimera(*25*). Prior to molecular dynamics simulation the protonation state of all residues were adjusted using H^{++} server(*26*) and the wrong residue flips were corrected to generate a reasonable starting structure.

Table 1

2.2. Molecular dynamics simulations

All systems were subjected to an all-atom molecular dynamics simulation using GPU version of PMEMD engine provided with Amber 14(*27*). A detailed reported of the system set up and simulation was provided in our previous reports (*28, 29*). In brief, the geometry of the ligands were optimized at HF/6-31G* level using Gaussian 09. Finally antechamber module was used in order to generate atomic partial charges for all the ligands using RESP and force field parameters of GAFF. The FF99SB force field

integrated with Amber 14 was used to describe the protein systems. The systems were then processed using typical parameters described by *Bhakat et al.*(*28*) and *Wilson et al.*(*29*). The minimization steps were performed using CPU version whereas the heating, equilibration steps were carried out using GPU version of Amber 14. Finally, MD production runs of 50ns each were accomplished using the GPU version of Amber 14 (*30*). The trajectories were saved in every 1 ps and analysed using the PTRAJ and CPPTRAJ modules (*31*) integrated within Amber 14. MM/GBSA based binding free energy calculations were performed using a singular trajectory approach averaged over 1000 snapshots at equal intervals of 50 ps as described in our previous reports(*28, 29, 32*). All plots were generated using data analysis software Origin(*33*).

3. Results and Discussion

3.1. Apo conformations ($Wild_{Apo}$ versus $Mutant_{Apo}$)

In a recent study, it was highlighted that the occurrence of T68A and N126Y mutations led to five-fold less susceptible to inhibitor than the wildtype virus as well as loss of conformation integrity on 3C protease of CVB3(*34*). Per-residue C-α fluctuation (RMSF) of $Wild_{Apo}$ and $Mutant_{Apo}$ show the presents of T68A/N126Y mutation led to an increased backbone fluctuation. The mutations at residue 68 and 126 resulted in an increased flexibility at those regions (**Table 2**) and surrounding regions (**Figure 3**). A possible explanation of this increased conformational flexibility is due to loss of residue-residue hydrogen bond connections.

Figure 3

Table 2

Commonly in other studies mutations led to an increased conformational flexibility due to loss of residue-residue hydrogen bond connections(*28*). Calculation of hydrogen bond counts between $Wild_{Apo}$ and $Mutant_{Apo}$ during simulation time (**Figure 4A**) highlights that average no. of H-bonds were slightly less in case of $Mutant_{Apo}$ (average no. of H-bonds 85) as compared to $Wild_{Apo}$ (average no. of H-bonds 87).

Figure 4

The calculations of radius of gyrations for $Wild_{Apo}$ and $Mutant_{Apo}$ were carried out at 300K as described in our previous reports *(28, 29)*. Radius of gyration (R_g) is defined as the moment of inertia of the C-α atoms from its centre of mass. The increased conformational flexibility led to destabilization in R_g. (**Figure 4B)** highlights difference in R_g fluctuation between $Wild_{Apo}$ and $Mutant_{Apo}$. The increased per-residue C-α fluctuation of $Mutant_{Apo}$ led to an increased average R_g (average R_g of $Mutant_{Apo}$ 15.46 Å) as compared to of the $Wild_{Apo}$ (15.40 Å). The trend of R_g further corroborated a conformational distortion hypothesis as a result of mutations, which contribute towards an increased conformational flexibility resulting a decreased the receptor grip on the inhibitor. An increased conformational flexibility in case of $Mutant_{Apo}$ (average SASA= 8150 $Å^2$) led to an increased average solvent accessible surface area (SASA) as compared to $Wild_{Apo}$ (average SASA=8144 $Å^2$) (**Figure 4C**). The trend in SASA, R_g and RMSF confirms that T68A/N126Y instigated an increased conformational flexibility mainly due to loss of residue-residue H-bond connections and possibly due to the loss of other residue-residue interaction forces.

The distorted landscape of $Wild_{Apo}$ and $Mutant_{Apo}$ further confirms that T68A/N126Y mutations led to a distorted protein conformation which ultimately affects proper binding of ligand due to a decreased receptor grip and ultimately resulted in drug resistance.

3.2. Bound conformations ($Wild_{Bound}$ versus $Mutant_{Bound}$)

3.2.1. Conformational analyses and ligand-binding landscape

As mentioned in the previous section (Section **3.1**) T68A/N126Y triggered an increased conformational flexibility that distorts the receptor grip on the ligand (3CPI), which ultimately leads to resistance. **Figure 5**, highlights the per-residue C-α fluctuation (RMSF) of $Wild_{Bound}$ and $Mutant_{Bound}$ conformations. The RMSF clearly demonstrate an overall increase in flexibility for $Mutant_{Bound}$ as compared to $Wild_{Bound}$. This phenomena is particularly prominent at the point of mutations, which ultimately affects the overall C-α fluctuation.

Figure 5

The increased RMSF fluctuation not only affects the overall conformational fluctuation but increases the fluctuation among active site residues (**Table 3**) which plays pivotal role in decreased inhibitor grip and subsequent drug resistance.

Table 3

As evident from section **3.1** and our previous reports, which stated that habitually mutations triggers a loss in residue-residue H-bond connections as well as ligand-residue H-bond connections. **Figure 6** and **Table 4** highlights the changes in residue-residue hydrogen bond network as well as ligand-residue hydrogen bond connections as a result of T68A/N126Y mutations. The loss in average residue-residue H-bond interactions and

ligand-residue H-bond interactions is in good agreement to the data's presented in section **3.1** and highlighted the reduced protein grip on ligand as a result of amplified conformational motion.

Figure 6

Table 4

Further, an in-depth analysis of ligand-residue hydrogen bond interactions (**Table 5**) highlighted a decreased % h-bond occupancy as well as an increased h-bond distance. A decreased % occupancy further confirms that T68A/N126Y double mutations led to distorted ligand binding landscape which resulted in a decreased protein grip on inhibitor as well as an increased average h-bond distance. A 2-D protein-ligand contact map (**Figure 9**7 taking in account average structure from each simulation also highlighted difference in protein-ligand contact map in a static state which also shows the distorted ligand interaction map in case of $Mutant_{Bound}$ as a results of T68A/N126Y double mutation.

Figure 7

Table 5

Further, analysis of R_g and SASA displayed a similar trend as described in section **3.1**. Both R_g and SASA (**Figure 8**) found to fluctuate more in case of $Mutant_{Bound}$ which further settle the fact that T68A/N126Y led to an increased conformational movement and decreased receptor grip on ligand as evident from an increased fluctuation in R_g and SASA.

Figure 8

3.2.2. Free energy profile

MM/GBSA based binding free energy analyses (**Table 6**) and per-residue energy decomposition has emerged as valuable tools to be applied in the understanding of the effect of mutations for the free energy profile of ligand binding. The T68A/N126Y mutations ($Mutant_{Bound}$) led to a lower ΔG_{bind} (~3 kcal/mol) when compared with wild type enzyme ($Wild_{Bound}$). The results are in agreement with the initial findings which states that protease with T68A/N126Y mutations are about five-fold less susceptible to the incoming inhibitor(*34*). Analyzing the corresponding energy contributions highlighted the fact that the van der Waals (vdW) contribution is the major driving force behind total binding energy. Both vdW and electrostatic contributions observed a decrease of ~1 kcal/mol each which contribute total a decrease in overall ΔG_{bind}.

Table 6

Per-residue energy decomposition revealed a slight decrease in energy contribution from particular active site residues, which confirms the negative effect of T68A/N126Y mutations on active site residues (**Figure 9**). It was also noticed that vdW and electrostatic energy contributions coming from residue 68 and 126 are lower for the $Mutant_{Bound}$ as compared to $Wild_{Bound}$ (**Table 7**).

Figure 9

Table 7

Principal component analyses of both apo and bound conformations highlighted significant difference in the motion as a result of mutations. From the PCA scatter plot presented in **Figure 10**, it is clear that eigenvectors computed from the MD trajectory for

$Wild_{Apo}$/$Mutant_{Apo}$; $Wild_{Bound}$/$Mutant_{Bound}$ systems are largely varied, which clearly indicates the difference in protein motions as a result of mutations.

Figure 10

The conformational analyses concerning the wild and mutant (Apo and bound) conformations forms of CVB3 3C protease has confirmed that the occupancy of T68A/N126Y mutations led to an overall increase in conformational flexibility. In addition it reduced receptor grip on the ligand. This was further validated by an increase in RMSF, Rg and SASA fluctuations both in the apo as well as in bound state. The mutations led to a change in 2-D ligand interaction map, residue-residue and ligand-residue H-bond interactions as well as decrease in binding free energy. These data's further validate the experimental findings, which justifies the development of resistance as a result of T68A/N126Y mutations.

4. Conclusion

The precise molecular level understanding of the serious impact of T68A/N126Y double mutations on inhibitor binding landscape is lacking in literature. In this report, we embarked on a wide range of computational approaches to provide a multidimensional view on the effect of the mutations mentioned above. Molecular dynamics simulations, binding free energy calculations, principle component analysis (PCA) and % occupancy led us to several findings that can explain the molecular level impact of T68A/N126Y double mutant. It is also noteworthy to mention that T68A/N126Y is believed to impact a number of structural changes in β-hairpin region of CVB3 3C protease(*35*). However to reveal those changes, the computational outcome should be combined with

crystallographic evidences and wet lab experiments. This study provides a firsthand computational understanding of the T68A/N126Y mutations and its effects on drug/ligand binding landscape targeting CVB3 3C protease. We believe this report will act as a benchmark for future *in-silico* or wet lab efforts to understand a more-detailed insight into structural changes across broad categories of CVB3 protease inhibitors. It will also assist towards structural based drug design efforts in order to combat the resistance caused by different type of mutations.

5. Conflict of Interests

Authors declare no potential conflict of interest

6. Acknowledgement

SB wish to thank Mr. Hezekiel Khumalo of School of Health Sciences, University of KwaZulu-Natal, Westville, Durban, South Africa for his support to carry out the calculations and other constructive discussions. Author also extends his thank to cBio cluster supported by MSKCC, USA for computational resources.

References

1. Barbani, M. T., and Gorgievski-Hrisoho, M. (2009) Rapid detection of respiratory picornaviruses in nasopharyngeal aspirates by immunofluorescence assay, *Journal of Clinical Virology 45*, 245-248.
2. Belov, G. A. (2014) Modulation of lipid synthesis and trafficking pathways by picornaviruses, *Current Opinion in Virology 9*, 19-23.
3. Feng, Q., Langereis, M. A., and van Kuppeveld, F. J. M. (2014) Induction and suppression of innate antiviral responses by picornaviruses, *Cytokine & Growth Factor Reviews 25*, 577-585.
4. Hirneisen, K., Reith, J. L., Wei, J., Hoover, D. G., Hicks, D. T., Pivarnik, L. F., and Kniel, K. E. (2014) Comparison of pressure inactivation of caliciviruses and

picornaviruses in a model food system, *Innovative Food Science & Emerging Technologies 26*, 102-107.
5. Nielsen, A. C. Y., Gyhrs, M. L., Nielsen, L. P., Pedersen, C., and Böttiger, B. (2013) Gastroenteritis and the novel picornaviruses aichi virus, cosavirus, saffold virus, and salivirus in young children, *Journal of Clinical Virology 57*, 239-242.
6. Bruning, A. H. L., Sanden, S. M. G. v. d., Hoedt, A. E. t., Wolthers, K. C., Kaam, A. H. v., and Pajkrt, D. (2015) An atypical course of coxsackievirus A6 associated hand, foot and mouth disease in extremely low birth weight preterm twins, *Journal of Clinical Virology 65*, 20-22.
7. Hou, W., Yang, L., He, D., Zheng, J., Xu, L., Liu, J., Liu, Y., Zhao, H., Ye, X., Cheng, T., and Xia, N. (2015) Development of a coxsackievirus A16 neutralization test based on the enzyme-linked immunospot assay, *Journal of Virological Methods 215–216*, 56-60.
8. Lim, B.-K., Yun, S.-H., Ju, E.-S., Kim, B.-K., Lee, Y.-J., Yoo, D.-K., Kim, Y.-C., and Jeon, E.-S. (2015) Soluble Coxsackievirus B3 3C Protease Inhibitor Prevents Cardiomyopathy in an Experimental Chronic Myocarditis Murine Model, *Virus Research 199*, 1-8.
9. Massilamany, C., Gangaplara, A., and Reddy, J. (2014) Intricacies of cardiac damage in coxsackievirus B3 infection: Implications for therapy, *International Journal of Cardiology 177*, 330-339.
10. Cunha, B. A., Mickail, N., and Petelin, A. P. (2012) Infectious mononucleosis-like syndrome probably attributable to Coxsackie A virus infection, *Heart & Lung: The Journal of Acute and Critical Care 41*, 522-524.
11. Gu, H.-S., Ma, S.-G., Li, Y.-H., Wang, Y.-D., Liu, Y.-B., Li, L., Li, Y., Qu, J., Lv, H.-N., Chen, X.-G., Jiang, J.-D., and Yu, S.-S. (2014) Claoxylones A–I, prenylbisabolane diterpenoids with anti-Coxsackie B virus activity from the branches and leaves of Claoxylon polot, *Tetrahedron 70*, 7476-7483.
12. Marsman, R. F. J., Bezzina, C. R., Freiberg, F., Verkerk, A. O., Adriaens, M. E., Podliesna, S., Chen, C., Purfürst, B., Spallek, B., Koopmann, T. T., Baczko, I., dos Remedios, C. G., George Jr, A. L., Bishopric, N. H., Lodder, E. M., de Bakker, J. M. T., Fischer, R., Coronel, R., Wilde, A. A. M., Gotthardt, M., and Remme, C. A. (2014) Coxsackie and Adenovirus Receptor Is a Modifier of Cardiac Conduction and Arrhythmia Vulnerability in the Setting of Myocardial Ischemia, *Journal of the American College of Cardiology 63*, 549-559.
13. Coudray-Meunier, C., Fraisse, A., Martin-Latil, S., Guillier, L., Delannoy, S., Fach, P., and Perelle, S. (2015) A comparative study of digital RT-PCR and RT-qPCR for quantification of Hepatitis A virus and Norovirus in lettuce and water samples, *International Journal of Food Microbiology 201*, 17-26.
14. Lodder, W. J., Schijven, J. F., Rutjes, S. A., de Roda Husman, A. M., and Teunis, P. F. M. (2015) Entero- and parechovirus distributions in surface water and probabilities of exposure to these viruses during water recreation, *Water Research 75*, 25-32.
15. (2012) Family - Picornaviridae, In *Virus Taxonomy* (King, A. M. Q., Adams, M. J., Carstens, E. B., and Lefkowitz, E. J., Eds.), pp 855-880, Elsevier, San Diego.

16. Wang, S., Huang, X., Zhang, J., and Huang, C. Antiviral and myocyte protective effects of IL-28A in coxsackievirus B3-induced myocarditis, *The Brazilian Journal of Infectious Diseases*.
17. Wu, F., Fan, X., Yue, Y., Xiong, S., and Dong, C. (2014) A vesicular stomatitis virus-based mucosal vaccine promotes dendritic cell maturation and elicits preferable immune response against coxsackievirus B3 induced viral myocarditis, *Vaccine 32*, 3917-3926.
18. Zhang, Y.-Y., Li, J.-N., Xia, H. H.-X., Zhang, S.-L., Zhong, J., Wu, Y.-Y., Miao, S.-K., and Zhou, L.-M. (2013) Protective effects of losartan in mice with chronic viral myocarditis induced by coxsackievirus B3, *Life Sciences 92*, 1186-1194.
19. Zell, R., Markgraf, R., Schmidtke, M., Görlach, M., Stelzner, A., Henke, A., Sigusch, H., and Glück, B. (2004) Nitric oxide donors inhibit the coxsackievirus B3 proteinases 2A and 3C in vitro, virus production in cells, and signs of myocarditis in virus-infected mice, *Med Microbiol Immunol 193*, 91-100.
20. Tong, L. (2002) Viral Proteases, *Chemical Reviews 102*, 4609-4626.
21. Lee, E. S., Lee, W. G., Yun, S.-H., Rho, S. H., Im, I., Yang, S. T., Sellamuthu, S., Lee, Y. J., Kwon, S. J., Park, O. K., Jeon, E.-S., Park, W. J., and Kim, Y.-C. (2007) Development of potent inhibitors of the coxsackievirus 3C protease, *Biochemical and Biophysical Research Communications 358*, 7-11.
22. Matthews, D. A., Dragovich, P. S., Webber, S. E., Fuhrman, S. A., Patick, A. K., Zalman, L. S., Hendrickson, T. F., Love, R. A., Prins, T. J., Marakovits, J. T., Zhou, R., Tikhe, J., Ford, C. E., Meador, J. W., Ferre, R. A., Brown, E. L., Binford, S. L., Brothers, M. A., DeLisle, D. M., and Worland, S. T. (1999) Structure-assisted design of mechanism-based irreversible inhibitors of human rhinovirus 3C protease with potent antiviral activity against multiple rhinovirus serotypes, *Proceedings of the National Academy of Sciences 96*, 11000-11007.
23. Norder, H., De Palma, A. M., Selisko, B., Costenaro, L., Papageorgiou, N., Arnan, C., Coutard, B., Lantez, V., De Lamballerie, X., Baronti, C., Solà, M., Tan, J., Neyts, J., Canard, B., Coll, M., Gorbalenya, A. E., and Hilgenfeld, R. (2011) Picornavirus non-structural proteins as targets for new anti-virals with broad activity, *Antiviral Research 89*, 204-218.
24. Honarparvar, B., Govender, T., Maguire, G. E. M., Soliman, M. E. S., and Kruger, H. G. (2014) Integrated Approach to Structure-Based Enzymatic Drug Design: Molecular Modeling, Spectroscopy, and Experimental Bioactivity, *Chemical Reviews 114*, 493-537.
25. Pettersen, E. F., Goddard, T. D., Huang, C. C., Couch, G. S., Greenblatt, D. M., Meng, E. C., and Ferrin, T. E. (2004) UCSF Chimera--a visualization system for exploratory research and analysis, *J Comput Chem 25*, 1605-1612.
26. Gordon, J. C., Myers, J. B., Folta, T., Shoja, V., Heath, L. S., and Onufriev, A. (2005) H++: a server for estimating pKas and adding missing hydrogens to macromolecules, *Nucleic Acids Res 33*, W368-371.
27. D.A. Case, V. Babin, J.T. Berryman, R.M. Betz, Q. Cai, D.S. Cerutti, T.E. Cheatham, III, T.A. Darden, R.E. Duke, H. Gohlke, A.W. Goetz, S. Gusarov, N. Homeyer, P. Janowski, J. Kaus, I. Kolossváry, A. Kovalenko, T.S. Lee, S. LeGrand, T. Luchko, R. Luo, B. Madej, K.M. Merz, F. Paesani, D.R. Roe, A.

Roitberg, C. Sagui, R. Salomon-Ferrer, G. Seabra, C.L. Simmerling, W. Smith, J. Swails, R.C. Walker, J. Wang, R.M. Wolf, X. Wu and P.A. Kollman (2014), AMBER 14, University of California, San Francisco.

28. Bhakat, S., Martin, A. J. M., and Soliman, M. E. S. (2014) An integrated molecular dynamics, principal component analysis and residue interaction network approach reveals the impact of M184V mutation on HIV reverse transcriptase resistance to lamivudine, *Molecular Biosystems 10*, 2215-2228.
29. Karubiu, W., Bhakat, S., and Soliman, M. S. (2014) Compensatory Role of Double Mutation N348I/M184V on Nevirapine Binding Landscape: Insight from Molecular Dynamics Simulation, *Protein J*, 1-15.
30. Case, D. A., Cheatham, T. E., Darden, T., Gohlke, H., Luo, R., Merz, K. M., Onufriev, A., Simmerling, C., Wang, B., and Woods, R. J. (2005) The Amber biomolecular simulation programs, *Journal of Computational Chemistry 26*, 1668-1688.
31. Roe, D. R., and Cheatham, T. E., III. (2013) PTRAJ and CPPTRAJ: Software for Processing and Analysis of Molecular Dynamics Trajectory Data, *Journal of Chemical Theory and Computation 9*, 3084-3095.
32. Bhakat, S., Chetty, S., Martin, A. J., and Soliman, M. E. (2015) Multi-drug Resistance Profile of PR20 HIV-1 Protease is attributed to Distorted Conformational and Drug Binding Landscape: Molecular Dynamics Insights, *J Biomol Struct Dyn 11*, 1-46.
33. http://www.originlab.com/.
34. profdoc.um.ac.ir/articles/a/1011455.pdf.
35. Norder, H., De Palma, A. M., Selisko, B., Costenaro, L., Papageorgiou, N., Arnan, C., Coutard, B., Lantez, V., De Lamballerie, X., Baronti, C., Sola, M., Tan, J., Neyts, J., Canard, B., Coll, M., Gorbalenya, A. E., and Hilgenfeld, R. (2011) Picornavirus non-structural proteins as targets for new anti-virals with broad activity, *Antiviral Res 89*, 204-218.
36. Laskowski, R. A., and Swindells, M. B. (2011) LigPlot+: multiple ligand-protein interaction diagrams for drug discovery, *J Chem Inf Model 51*, 2778-2786.
37. http://www.rcsb.org/pdb/explore.do?structureId=3ZYD.
38. http://www.rcsb.org/pdb/explore.do?structureId=3ZZ4.
39. http://www.rcsb.org/pdb/explore.do?structureId=3ZZ9.
40. http://www.rcsb.org/pdb/explore.do?structureId=3ZZC.

List of Figures

Figure 1. Representation of CVB3 genome and several domains, which constituted its architecture.

Figure 2. Representation of Wild (cornflower blue) and T68A/N126Y (magenta) conformations of CVB3 3C protease. Residues at 68 and 126 were zoomed in for better understanding.

Figure 3. Per-residue C-α fluctuations of $Wild_{Apo}$ and $Mutant_{Apo}$ during simulation time. The fluctuations at mutational sites T68A (blue) and N126Y (orange) were highlighted which showed an increased fluctuation as a result of mutation.

Figure 4. Fluctuation in residue-residue H-bond occupancy (**A**), R_g (**B**) and SASA (**C**) during simulation time for $Wild_{Apo}$ and $Mutant_{Apo}$ conformations of CVB3 3C protease.

Figure 5. Per-residue C-α fluctuations of $Wild_{Bound}$ and $Mutant_{Bound}$ during simulation time. The fluctuations at mutational sites T68A (blue) and N126Y (orange) were highlighted which showed an increased fluctuation as a result of mutation.

Figure 6. Fluctuation in number of residue-residue (A) and ligand-residue (B) hydrogen bond interactions during simulation time for $Wild_{Bound}$ and $Mutant_{Bound}$ during simulation time.

Figure 7. The relative position of ligand (3CPI) inside the active site of $Wild_{Bound}$ (cornflower blue) and $Mutant_{Bound}$ (orange) taking in account average PDB structure from

each simulation (**A**). **B** and **C** highlights 2-D ligand interaction map for $Wild_{Bound}$ and $Mutant_{Bound}$ respectively. Ligand interaction plots were generated using LigPlot^{+}(*36*).

Figure 8. Fluctuation of R_g and SASA during simulation time for $Wild_{Bound}$ and $Mutant_{Bound}$ conformations. The average Rg fluctuation found to be 15.45 Å and 15.50 Å respectively for $Wild_{Bound}$ and $Mutant_{Bound}$ whereas average SASA was reported to be 8151 $Å^2$ and 8407 $Å^2$ respectively for $Wild_{Bound}$ and $Mutant_{Bound}$.

Figure 9. Per-residue energy decomposition analysis for $Wild_{Bound}$ and $Mutant_{Bound}$ conformations of CVB3 3C protease.

Figure 10. Projection of PC1 over PC2 for apo and bound conformations of CVB3 3C protease.

List of Tables

Table 1. The systems used for simulation study with their PDB codes and abbreviations

Table 2. RMSF fluctuation(s) corresponding to certain region of $Wild_{Apo}$ and $Mutant_{Apo}$.

Table 3. RMSF fluctuation(s) corresponding to certain region/s of $Wild_{Bound}$ and $Mutant_{Bound}$.

Table 4. Average number of residue-residue and ligand-residue hydrogen bond interactions during simulation time for $Wild_{Bound}$ and $Mutant_{Bound}$ systems.

Table 5. % occupancy and average distance (Å) between ligand (3CPI) and prominent active site residues were calculated over simulation time. A complete list of all interactions were presented in supplementary materials.

Table 6. MM/GBSA binding free energy profile of wild ($Wild_{Bound}$) and T68A/N126Y ($Mutant_{Bound}$) variant of 3C protease of CVB3 complexed with the inhibitor. All energy terms are presented in *kcal/mol* unit.

Table 7. Per-residue binding free energy profile of $Wild_{Bound}$ and $Mutant_{Bound}$ conformations.

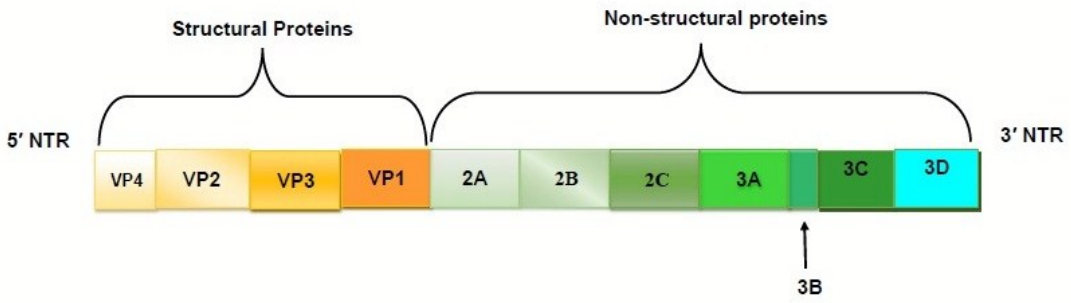

Figure 1. Representation of CVB3 genome and several domains, which constituted its architecture.

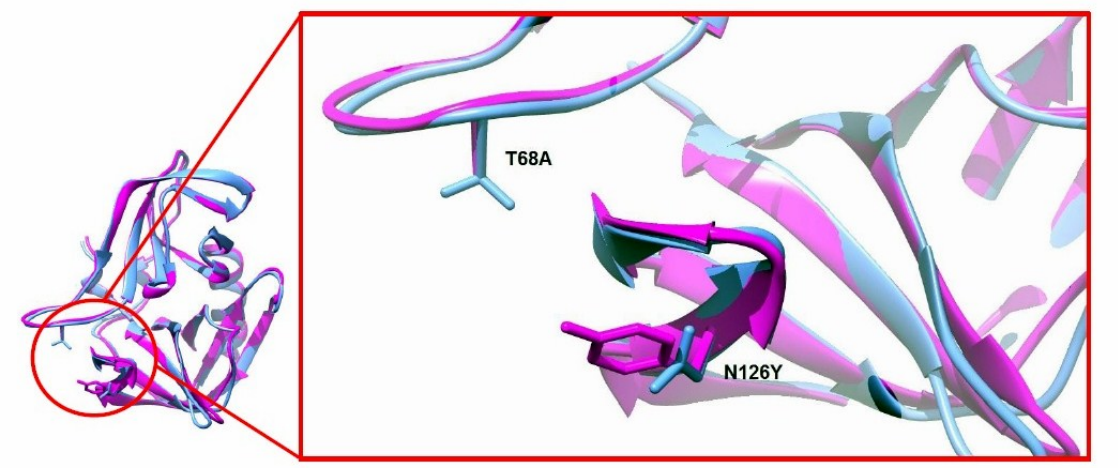

Figure 2. Representation of Wild (cornflower blue) and T68A/N126Y (magenta) conformations of CVB3 3C protease. Residues at 68 and 126 were zoomed in for better understanding.

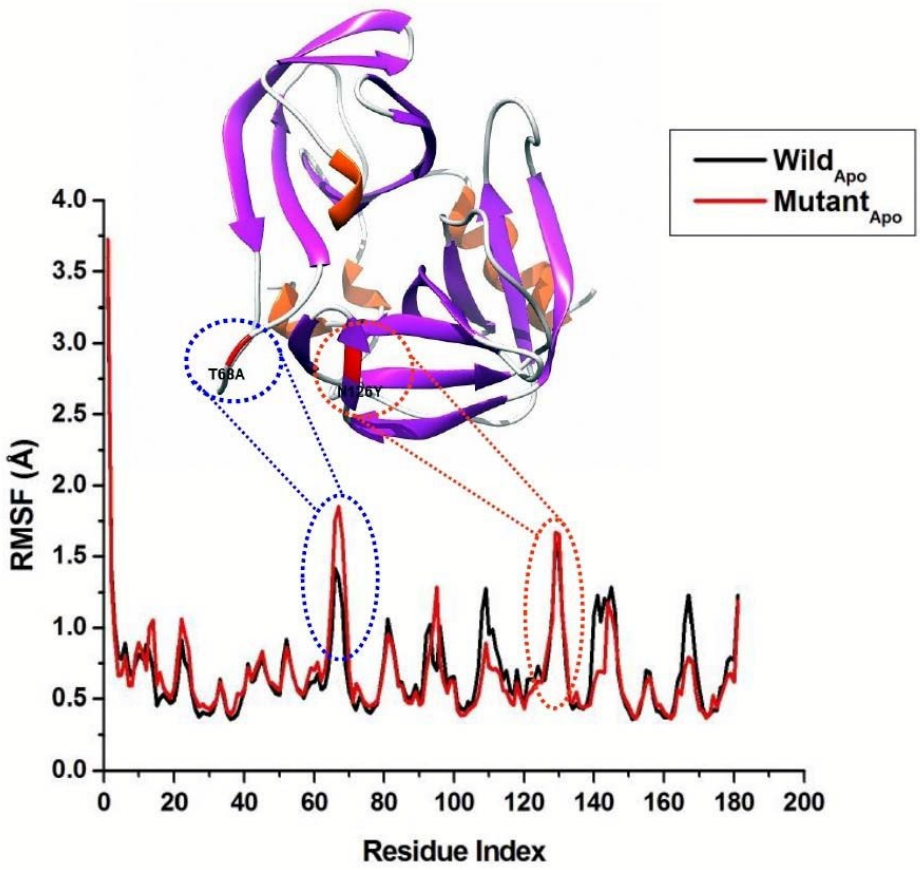

Figure 3. Per-residue C-α fluctuations of $Wild_{Apo}$ and $Mutant_{Apo}$ during simulation time. The fluctuations at mutational sites T68A (blue) and N126Y (orange) were highlighted which showed an increased fluctuation as a result of mutation.

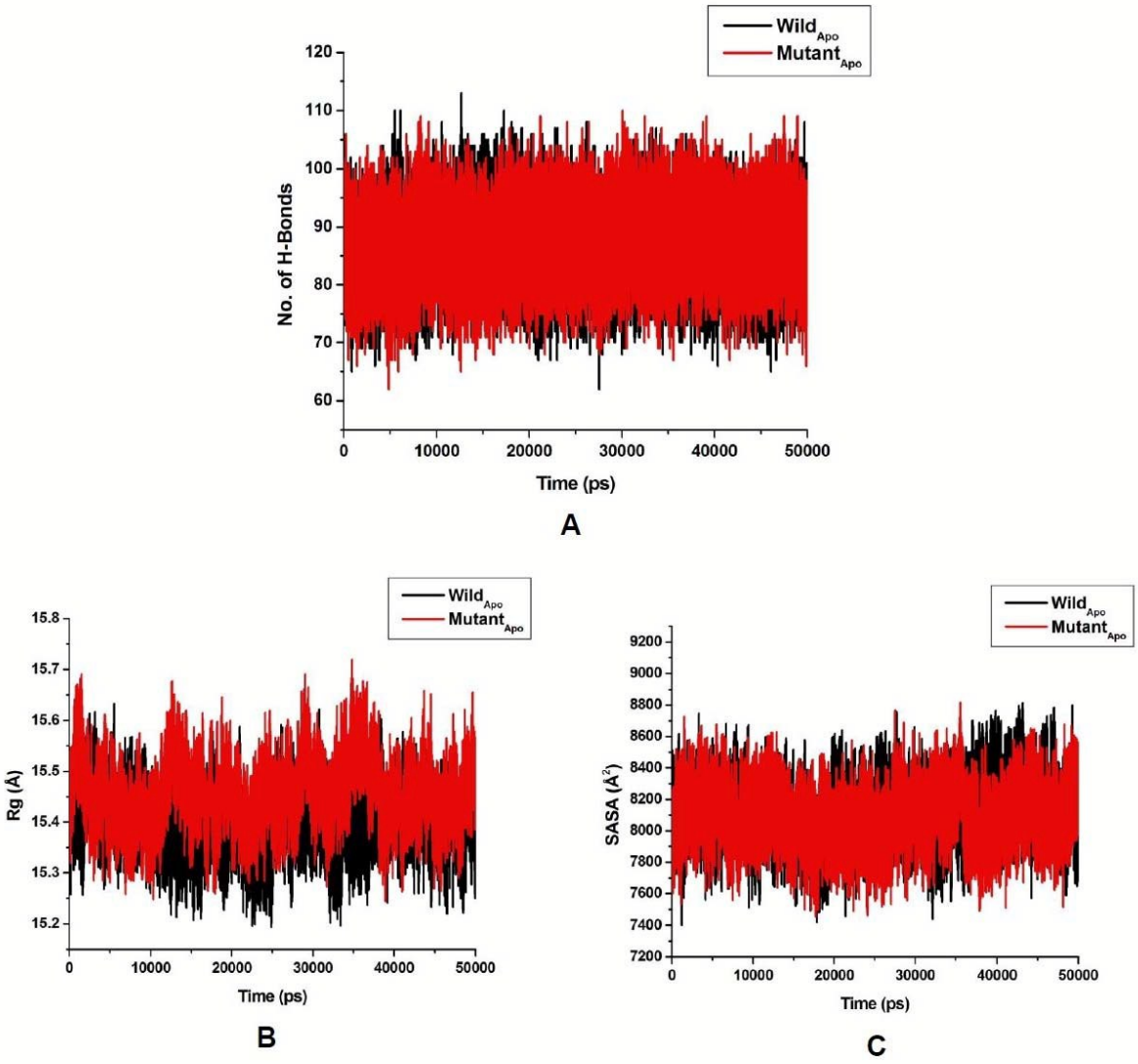

Figure 4. Fluctuation in residue-residue H-bond occupancy (**A**), R_g (**B**) and SASA (**C**) during simulation time for $Wild_{Apo}$ and $Mutant_{Apo}$ conformations of CVB3 3C protease.

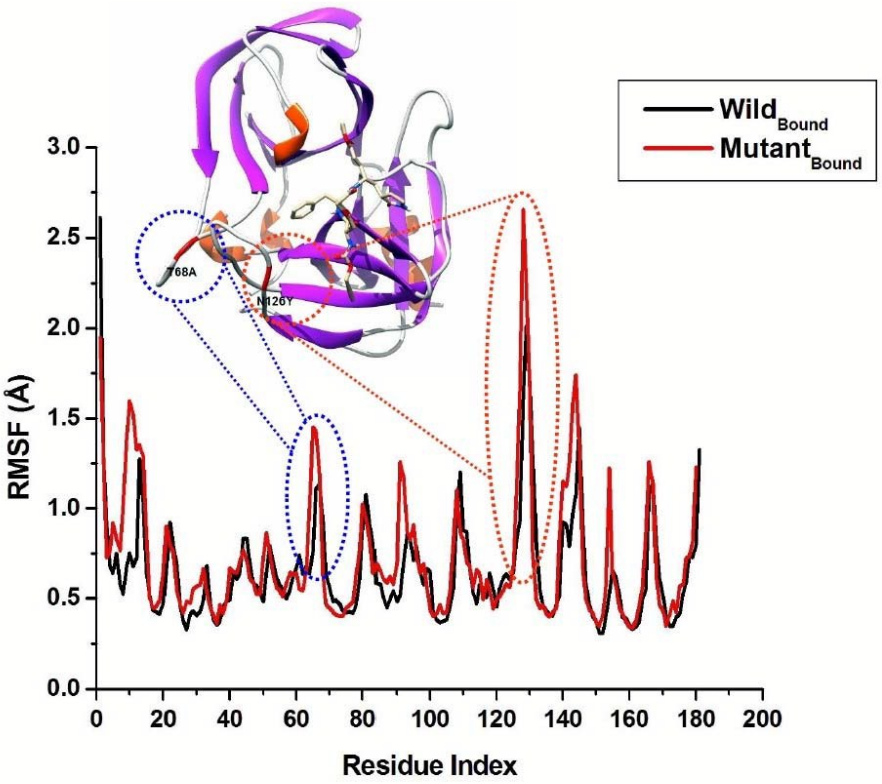

Figure 5. Per-residue C-α fluctuations of $Wild_{Bound}$ and $Mutant_{Bound}$ during simulation time. The fluctuations at mutational sites T68A (blue) and N126Y (orange) were highlighted which showed an increased fluctuation as a result of mutation.

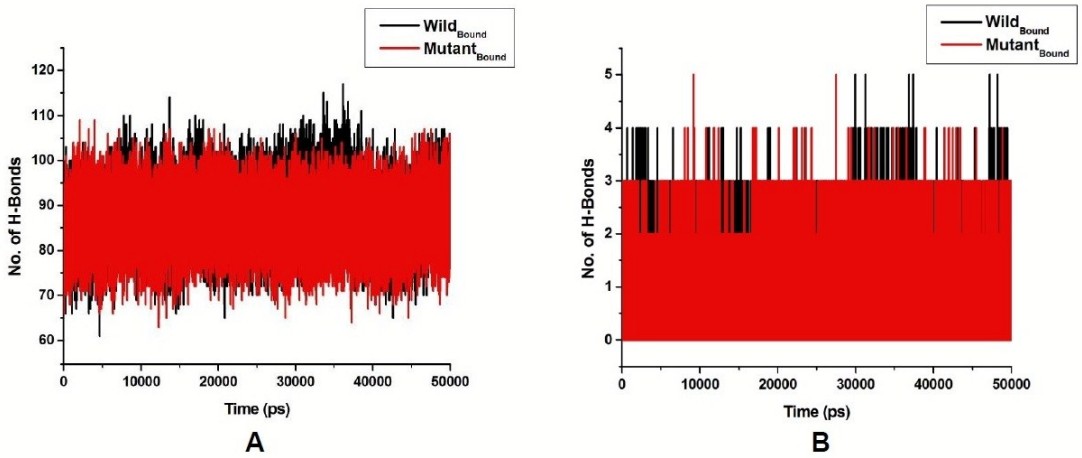

Figure 6. Fluctuation in number of residue-residue (A) and ligand-residue (B) hydrogen bond interactions during simulation time for $Wild_{Bound}$ and $Mutant_{Bound}$ during simulation time.

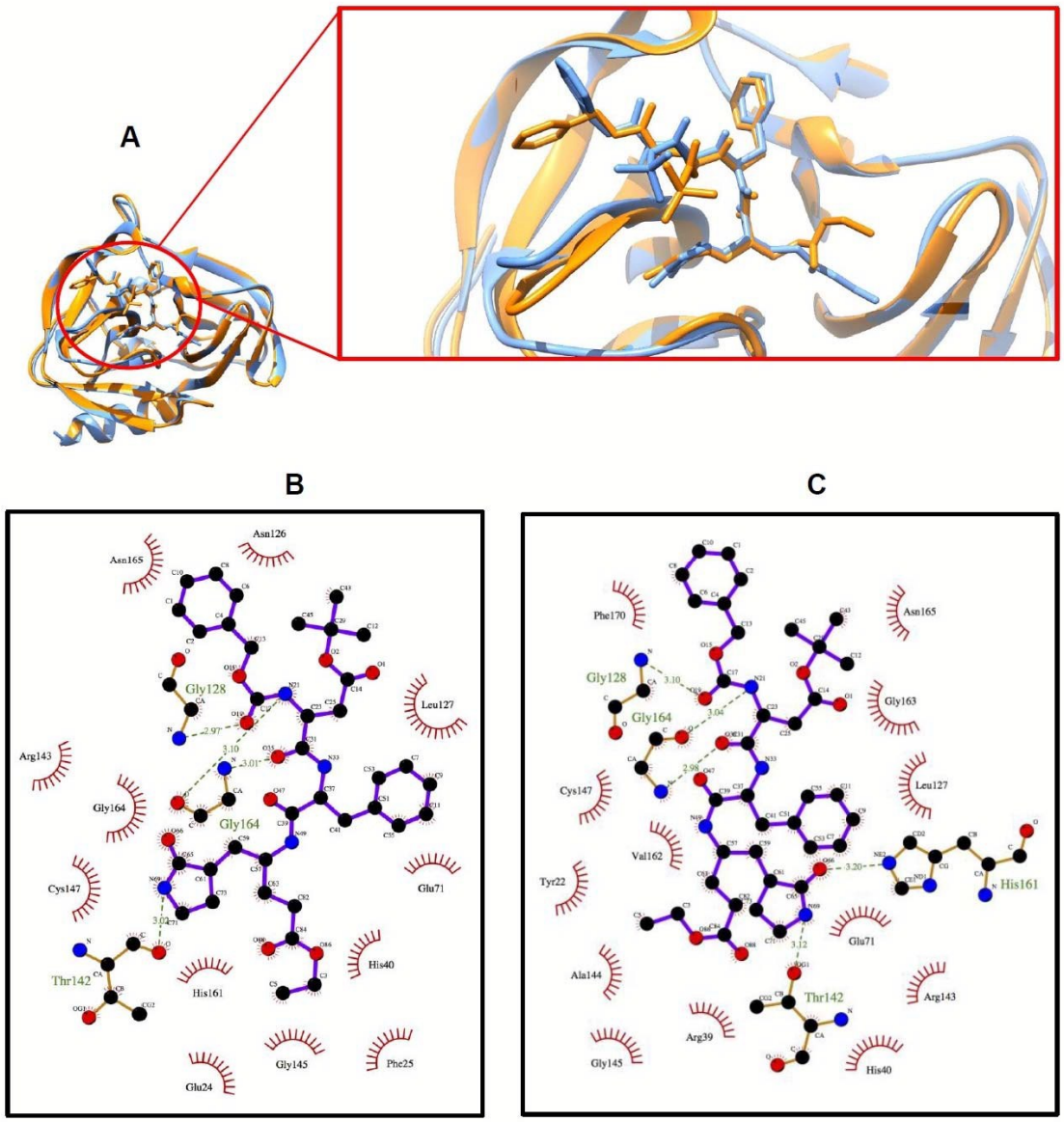

Figure 7. The relative position of ligand inside the active site of $Wild_{Bound}$ (cornflower blue) and $Mutant_{Bound}$ (orange) taking in account average PDB structure from each

simulation (**A**). **B** and **C** highlights 2-D ligand interaction map for $Wild_{Bound}$ and $Mutant_{Bound}$ respectively. Ligand interaction plots were generated using LigPlot^{+}(*36*).

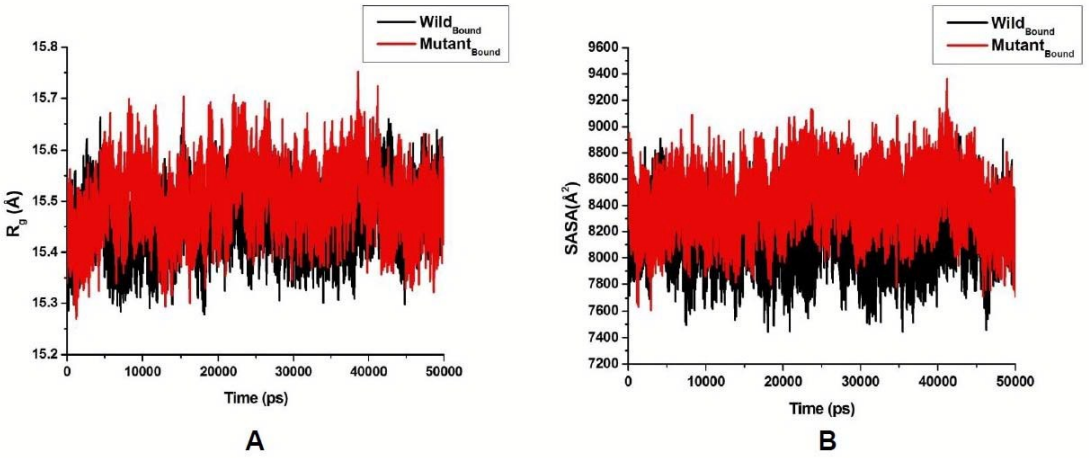

Figure 8. Fluctuation of R_g and SASA during simulation time for $Wild_{Bound}$ and $Mutant_{Bound}$ conformations. The average R_g fluctuation found to be 15.45 Å and 15.50 Å respectively for $Wild_{Bound}$ and $Mutant_{Bound}$ whereas average SASA was reported to be 8151 Å^2 and 8407 Å^2 respectively for $Wild_{Bound}$ and $Mutant_{Bound}$.

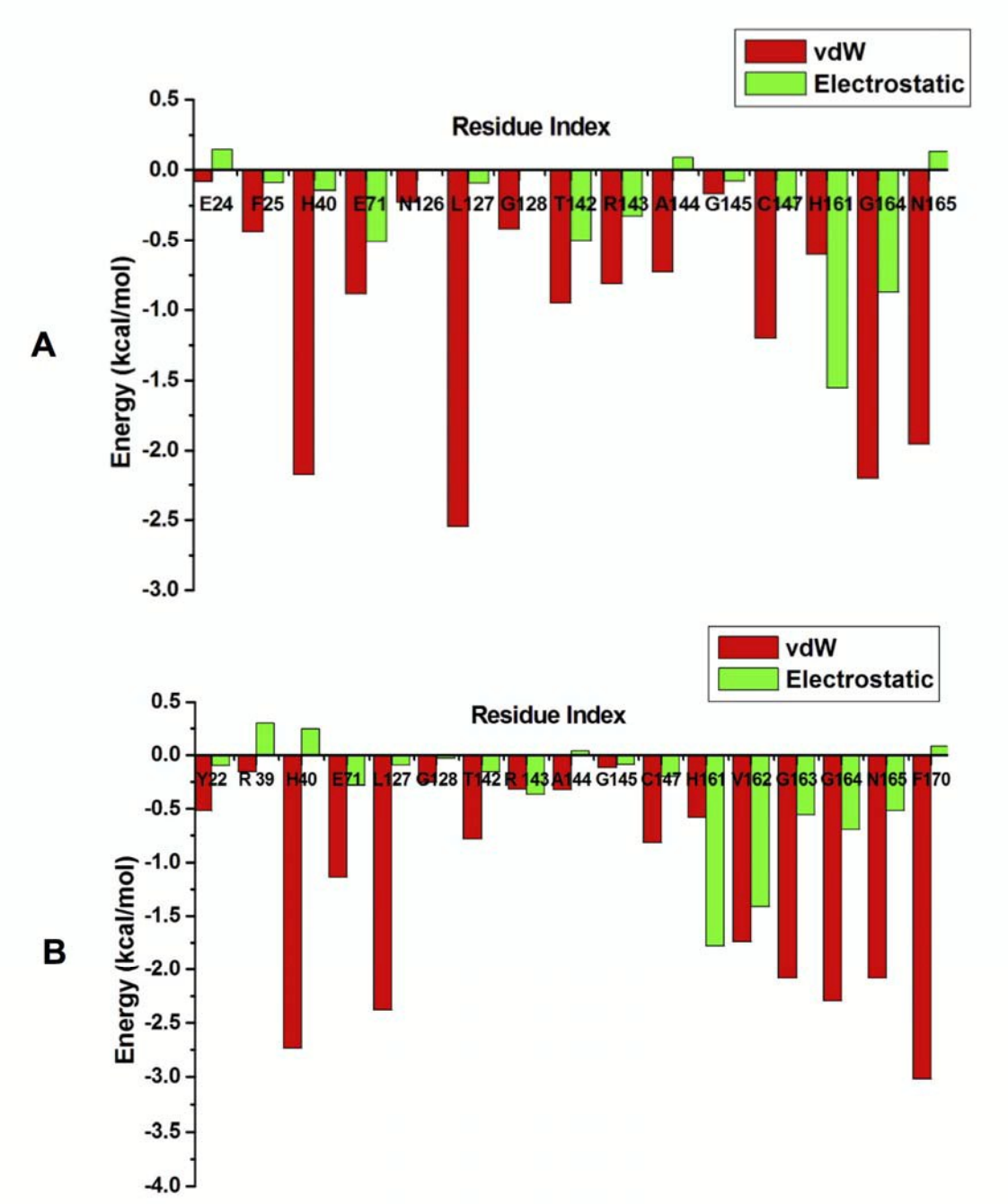

Figure 9. Per-residue energy decomposition analysis for $Wild_{Bound}$ and $Mutant_{Bound}$ conformations of CVB3 3C protease.

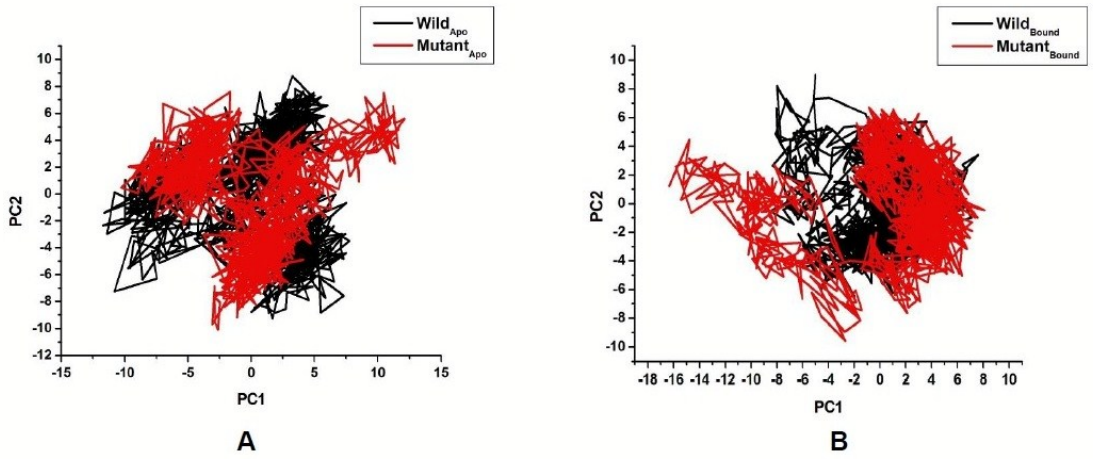

Figure 10. Projection of PC1 over PC2 for apo and bound conformations of CVB3 3C protease.

Table 1. The systems used for simulation study with their PDB codes and abbreviations

Systems	PDB Codes	Abbreviations
Wild 3C protease CVB3	3ZYD(*37*)	$Wild_{Apo}$
Mutant (T68A/N126Y) 3C protease CVB3	3ZZ4(*38*)	$Mutant_{Apo}$
Wild 3C protease CVB3+ ligand (3CPI)	3ZZ9(*39*)	$Wild_{Bound}$
Mutant (T68A/N126Y) 3C protease CVB3+ ligand (3CPI)	3ZZC(*40*)	$Mutant_{Bound}$

Table 2. RMSF fluctuation(s) corresponding to certain region of $Wild_{Apo}$ and $Mutant_{Apo}$.

Residue(s)	$Wild_{Apo}$	$Mutant_{Apo}$
68	1.21 Å	1.63 Å
126	0.64 Å	0.74 Å
60-80	0.68 Å*	0.82 Å*
125-135	0.86 Å*	0.91 Å*

*average RMSF fluctuation

Table 3. RMSF fluctuation(s) corresponding to certain region/s of $Wild_{Bound}$ and $Mutant_{Bound}$.

Residue(s)	$Wild_{Bound}$	$Mutant_{Bound}$
68	0.62 Å	1.19 Å
126	0.80 Å	1.07 Å
40, 127-162§	0.68 Å*	0.82 Å*

§ active site residues; * average RMSF values

Table 4. Average number of residue-residue and ligand-residue hydrogen bond interactions during simulation time for $Wild_{Bound}$ and $Mutant_{Bound}$ systems.

Systems	No. of residue-residue H-bond connections¶	No. of ligand-residue H-bond interactions¶
$Wild_{Bound}$	89	0.97
$Mutant_{Bound}$	86	0.81

¶ average value

Table 5. % occupancy and average distance (Å) between ligand and prominent active site residues were calculated over simulation time. A complete list of all interactions were presented in supplementary materials.

Acceptor	DonorH	Donor	% Occupancy $Wild_{Bound}$	% Occupancy $Mutant_{Bound}$	Avg. Distance (Å) $Wild_{Bound}$	Avg. Distance (Å) $Mutant_{Bound}$
G83@O35	Gly164@H	Gly165@N	50.44%	38.40%	2.885	2.895
G83@O66	His161@HE2	His161@NE2	13.26%	26.37%	2.882	2.893
Val162@O	G83@H49	G83@N49	12.88%	5.10%	2.917	2.930
Gly164@O	G83@H21	G83@N21	9.47%	1.55%	2.912	2.924
Arg143@O	G83@H69	G83@N69	8.26%	0.35%	2.902	2.899
G83182@O66	Thr142@HG1	Thr142@OG1	1.02%	0.42%	2.848	2.843
Thr142@O	G83@H69	G83@N69	0.98%	0.05%	2.913	2.909
Thr142@OG1	G83@H69	G83@N69	0.77%	1.34%	2.931	2.932
G83@O86	Gly145@H	Gly145@N	0.50%	0.08%	2.917	2.902

Table 6. MM/GBSA binding free energy profile of wild ($Wild_{Bound}$) and T68A/N126Y ($Mutant_{Bound}$) variant of 3C protease of CVB3 complexed with the inhibitor. All energy terms are presented in *kcal/mol* unit.

Systems	E_{vdw}	E_{elec}	ΔG_{solv}	ΔG_{gas}	ΔG_{bind}
Wild	-60.3557±0.3660	-12.3396±0.3174	21.4138±0.2285	-72.6952±0.4561	-51.2814±0.3806
T68A/N126Y	-59.3494±0.4845	-11.5533±0.2325	22.8675±0.2458	-73.9016±0.5132	-48.0341±0.4988

Table 7. Per-residue binding free energy profile of $Wild_{Bound}$ and $Mutant_{Bound}$ conformations.

Residues	vdW (kcal/mol)	Electrostatic (kcal/mol)
Thr68	-0.009±0.002	0.014±0.007
Ala68*	-0.007±0.002*	0.019±0.008*
Asn126	-0.226±0.165	0.004±0.115
Tyr126*	-0.173±0.128*	0.055±0.085*

*T68A/N126Y mutant